



Molecular recognition of trehalose and trehalose analogues by *Mycobacterium tuberculosis* LpqY-SugABC

Jingxi Liang^{a,b,1}, Fengjiang Liu^{c,1}, Peng Xu^d, Wei Shangguan^d, Tianyu Hu^b, Shule Wang^b, Xiaolin Yang^b, Zhiqi Xiong^e, Xiuna Yang^{b,f}, Luke W. Guddat^g, Biao Yu^{d,2}, Zihao Rao^{a,b,c,e,f,2}, and Bing Zhang^{b,f,2}

Edited by Dinshaw Patel, Memorial Sloan Kettering Cancer Center, New York, NY; received May 6, 2023; accepted July 25, 2023

Trehalose plays a crucial role in the survival and virulence of the deadly human pathogen *Mycobacterium tuberculosis* (*Mtb*). The type I ATP-binding cassette (ABC) transporter LpqY-SugABC is the sole pathway for trehalose to enter *Mtb*. The substrate-binding protein, LpqY, which forms a stable complex with the translocator SugABC, recognizes and captures trehalose and its analogues in the periplasmic space, but the precise molecular mechanism for this process is still not well understood. This study reports a 3.02-Å cryoelectron microscopy structure of trehalose-bound *Mtb* LpqY-SugABC in the pretranslocation state, a crystal structure of *Mtb* LpqY in a closed form with trehalose bound and five crystal structures of *Mtb* LpqY in complex with different trehalose analogues. These structures, accompanied by substrate-stimulated ATPase activity data, reveal how LpqY recognizes and binds trehalose and its analogues, and highlight the flexibility in the substrate binding pocket of LpqY. These data provide critical insights into the design of trehalose analogues that could serve as potential molecular probe tools or as anti-TB drugs.

trehalose | trehalose analogue | LpqY-SugABC | ABC transporter | *Mycobacterium tuberculosis*

Tuberculosis (TB), caused by *Mycobacterium tuberculosis* (*Mtb*), remains a global threat to human health (1). *Mtb* is a successful pathogen that has adapted well within the human host. This is due to its glycolipid-rich mycomembrane that acts as a barrier to prevent the entry of antibiotics, participates in the immune response, and also helps *Mtb* survive in macrophages (2, 3). Because of the importance of the mycomembrane, the proteins involved in the biosynthesis pathways of its components are good targets for developing anti-TB drugs (4, 5).

Trehalose (α -D-glucopyranosyl- α -D-glucopyranoside), a nonreducing nonmammalian disaccharide, acts as a “scaffold” for many trehalose-containing glycolipids such as trehalose monomycolate (TMM) and trehalose dimycolate (TDM; cord factor) (6–8). These trehalose-containing glycolipids are vitally important for the survival and pathogenicity of *Mtb*, because some of them are precursors of the core components of the cell wall and the others directly participate in mediating the host immune response (3, 6, 9). Of note, the transporter LpqY-SugABC is the sole pathway for trehalose and its analogues to enter the cytoplasm of *Mtb* as well as other mycobacteria (10–12). Intriguingly, for the synthesis of TDM and the core component of the *Mtb* cell wall, mycolic acids, the precursor TMM, synthesized in the cytoplasm, needs to be transported to the periplasm by the mycolic acids transporter MmpL3 (13, 14). Subsequently in the periplasmic space, TMM is processed by mycolyltransferase antigen 85 (Ag85) to arabinogalactan mycolates (AGM) or TDM and these then release trehalose (15, 16). The released trehalose is then recycled by the LpqY-SugABC system (10). More importantly, the disruption of trehalose recycling strongly impairs virulence of *Mtb* and also attenuates *Mtb* growth in human macrophages (10). In addition, normal trehalose recycling alleviates the energetic burden of mycomembrane remodeling under carbon limitation (17). Currently, trehalose analogues have already shown to have great potential as antibacterial agents, and can inhibit the growth and the formation of biofilms in mycobacteria (11). In addition, trehalose analogues also can be used as molecular probe tools for imaging and detection of live mycobacteria in vitro, in macrophages or in sputum samples from TB patients (12, 18–23).

In this recycling system, LpqY is a substrate-binding protein (SBP) that can capture trehalose via a “Venus fly-trap mechanism”, while LpqY can anchor to the inner membrane by an N-terminal lipid modification and form a stable complex with the translocator SugABC (24–26). SugA and SugB containing a total of 12 transmembrane helices form the transmembrane domain (TMD) and harbor a substrate translocation pathway between these two subunits; two SugC molecules with nucleotide-binding

Significance

Mycobacterium tuberculosis (*Mtb*) infection poses a serious threat to human health and results in more than one million deaths annually. There is thus an urgent need to develop new therapeutic drugs and detection methods to deal with the current tuberculosis epidemic. Trehalose is essential for the survival and pathogenicity of *Mtb*, and its analogues have already shown to have great potential as antibacterial agents and molecular probe tools. Here, we reveal how the trehalose-specific importer LpqY-SugABC of *Mtb* recognizes and binds trehalose and its analogues. These data pave the way for further rational structure-based design of trehalose analogues, and facilitate the application of trehalose analogues for the diagnosis or treatment of tuberculosis.

Author contributions: Z.R., B.Z., and B.Y. designed research; J.L., F.L., P.X., W.S., T.H., S.W., Xiaolin Yang, Z.X., and Xiuna Yang performed research; J.L., F.L., L.W.G., and B.Z. analyzed data; and B.Z., J.L., F.L., L.W.G., and Z.R. wrote the paper.

The authors declare no competing interest.

This article is a PNAS Direct Submission.

Copyright © 2023 the Author(s). Published by PNAS. This open access article is distributed under Creative Commons Attribution-NonCommercial-NoDerivatives License 4.0 (CC BY-NC-ND).

¹J.L. and F.L. contributed equally to this work.

²To whom correspondence may be addressed. Email: byu@sioc.ac.cn, raozh@tsinghua.edu.cn, or zhangbing@shanghaiitech.edu.cn.

This article contains supporting information online at <https://www.pnas.org/lookup/suppl/doi:10.1073/pnas.2307625120/-DCSupplemental>.

Published August 21, 2023.

domains (NBDs) form a dimer, which bind and hydrolyze ATP to provide the power for the conformational changes of the whole complex during the transport process (26). Recently, our group determined four cryoelectron microscope (cryo-EM) structures of *Mycobacterium smegmatis* LpqY-SugABC (*Ms* LpqY-SugABC) and unveiled an alternating access mechanism for trehalose transport across the mycobacterial membrane (26). In addition, the crystal structures of *Mtb* LpqY in an *apo* and open-liganded form were also determined (27). However, the precise molecular mechanism as to how *Mtb* LpqY specifically recognizes trehalose and its analogues is still largely unknown.

Herein, we have determined a 3.02-Å cryo-EM structure of *Mtb* LpqY-SugABC in complex with trehalose in the pretranslocation state, a crystal structure of *Mtb* LpqY with trehalose bound in a close-liganded form, and five crystal structures of *Mtb* LpqY in complex with different trehalose analogues. Our structural information combined with functional data explains how *Mtb* LpqY-SugABC recognizes and captures trehalose and its analogues.

Results

Molecular Basis for Trehalose Recognition by *Mtb* LpqY-SugABC.

To determine the structure of *Mtb* LpqY-SugABC in complex with trehalose, we overexpressed the *Mtb* LpqY-SugABC complex in *M. smegmatis* and purified it with lauryl maltose neopentyl glycol (LMNG) detergent (*SI Appendix*, Fig. S1A). Before freezing the sample, the detergent was changed to glyco-diosgenin (GDN), and an additional 2 mM trehalose was added into the protein sample incubating on ice. After cryo-EM data collection and processing, a 3.02-Å cryo-EM map of *Mtb* LpqY-SugABC in complex with trehalose (LpqY-SugABC_{TRE}) was obtained (Fig. 1 and *SI Appendix*, Fig. S2). The overall structure of *Mtb* LpqY-SugABC_{TRE} is largely identical with the structure of *M. smegmatis* LpqY-SugABC with trehalose bound (*Ms* LpqY-SugABC_{TRE}, PDB code:7CAF) with a rmsd of 1.67 Å for 1,626 aligned Cα atoms (*SI Appendix*, Fig. S3A).

In this state, LpqY presents a closed liganded conformation with a trehalose bound and docks tightly to the TMD of SugABC

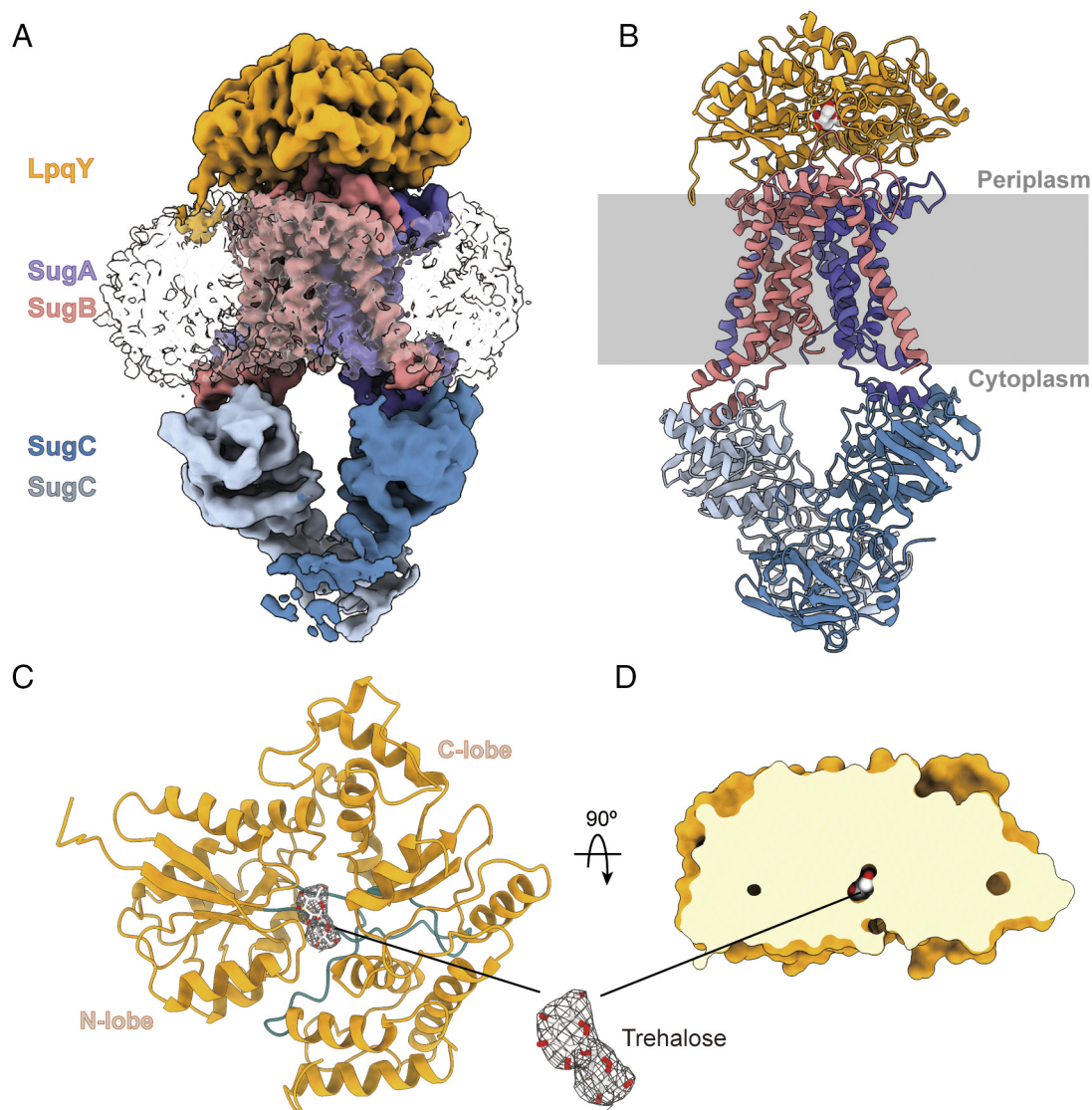


Fig. 1. Cryo-EM structure of LpqY-SugABC in complex with trehalose from *Mtb*. (A) Cryo-EM map of *Mtb* LpqY-SugABC bound trehalose (LpqY-SugABC_{TRE}) at 3.02 Å resolution. The detergent micelle around SugA and SugB is in white. (B) Cartoon representation of *Mtb* LpqY-SugABC_{TRE} viewed from the plane of the membrane. The membrane is shown in grey. LpqY is colored orange, and trehalose is shown white and red spheres. SugA and SugB are in slate blue and light coral, respectively. SugC is colored steel blue or light steel blue. (C) Cartoon representation of the trehalose-bound structure of *Mtb* LpqY. LpqY is divided into two parts (N-lobe and C-lobe) and the hinge regions (teal) connect the two lobes as indicated. The atomic model of trehalose with its cryo-EM density shown with the threshold of the map being 0.33. (D) Surface representation of *Mtb* LpqY that has been cross-sectioned at the point where trehalose is bound.

(Fig. 1). Trehalose is bound in a groove between the N- and C-lobes of LpqY, and its binding pocket is clearly defined in the cryo-EM density. Due to trehalose being formed by two glucopyranosyl units linked to each other by a α 1,1-glycosidic bond, we present the two glucose moieties of trehalose as Glc-1 and Glc-2. In LpqY, the Glc-1 moiety is buried at the base of the binding pocket near to the hinge region containing Arg421, whereas the Glc-2 moiety extends outward toward the entrance of the binding cleft (Fig. 2A and B). The two glucose moieties of trehalose are stabilized in the substrate-binding pocket of LpqY mainly through an extensive network of hydrogen bonds in which all hydroxyl groups of trehalose participate (Fig. 2). Specifically, the side chains of Arg421 and Asp97 both interact with the O3 and O4 of Glc-1. The O6 hydroxyl group of Glc-1 is orientated to interact with the side chain of Glu258. Notably, the side chain of Asn151 in the hinge region

interacts with the both Glc-1 and Glc-2 through the O2 of Glc-1 and the O6 of Glc-2, respectively. The O2, O3, and O4 hydroxyl groups of Glc-2 make interactions with the side chains of Gln76, Thr42, and Asp43, respectively. Moreover, the stacking interaction of Trp276 with Glc-1 provides additional stabilization for trehalose binding. A sequence comparison analysis of the binding cavity in LpqY shows that almost all residues involved in trehalose binding are conserved in all homologs, except that Thr42 can change to asparagine and Asp43 can change to glutamate (27).

Substrate-stimulated ATPase activity is a feature of ABC transporters (28–30). Previously, we have suggested trehalose as a substrate for the LpqY-SugABC system can stimulate LpqY-SugABC ATPase activity in a similar fashion to that observed in the *Escherichia coli* maltose transporter MalEFGK₂ (31). As expected, the transporter LpqY-SugABC shows a substrate stimulated ATPase activity with an ~14-fold increase following the addition of trehalose in the detergent condition (Fig. 2D). In contrast, maltose (4-O- α -D-glucopyranosyl- β -D-glucopyranose) and β , β -trehalose (β -D-glucopyranosyl- β -D-glucopyranoside) do not stimulate ATPase activity of LpqY-SugABC (see Fig. 4B), which is consistent with the fact that this system is a trehalose-specific importer (10).

To reveal the functional importance of trehalose-coordinating residues in LpqY, we generated eight LpqY-SugABC point mutation variants designed to disturb trehalose binding, including D97A, E258A, and R421A designed to disrupt the polar interactions with the Glc-1 moiety; T42A, D43A, and Q76A designed to disrupt the polar interactions with the Glc-2 moiety; N151A designed to disrupt the polar interactions with the both Glc-1 and Glc-2 moieties; and W276A designed to disrupt the hydrophobic interactions with the Glc-1 moiety. All variants displayed similar expression levels after affinity purification (SI Appendix, Fig. S1C). As was observed for the wild-type (WT) LpqY-SugABC, all LpqY mutants retained their trehalose-induced stimulation, but their ATPase activities were drastically diminished except for T42A (Fig. 2D), highlighting the importance of these residues for trehalose binding. Although Asp43 in *Mtb* LpqY is replaced by glutamate in all of its homologs, the key acidic interactions that are necessary to stabilize the Glc-2 moiety are conserved.

Crystal Structure of *Mtb* LpqY with Trehalose Bound in a Closed Liganded Form. We also overexpressed and purified the individual *Mtb* LpqY subunit (SI Appendix, Fig. S1B) and solved the co-crystal structure of *Mtb* LpqY in complex with trehalose (LpqY_{TRE}) at 1.50-Å resolution (Fig. 3A and SI Appendix, Fig. S4A). The electron density of the trehalose molecule is clearly found in the binding pocket of LpqY (SI Appendix, Fig. S4A). In addition, we also found six extra densities in this complex, two of which are near the trehalose binding pocket (SI Appendix, Fig. S4A). Considering 1.6 M lithium sulfate monohydrate was in the crystallization reservoir solution, it is most likely that sulfate ions could fit into these densities (SI Appendix, Fig. S4A). The crystal structure of *Mtb* LpqY_{TRE} is nearly identical with the overall structure of LpqY in the cryo-EM complex structure (*Mtb* LpqY-SugABC_{TRE}) with an RMSD of 0.883 Å for the 411 aligned C α atoms (Fig. 3A). However, this structure is significantly different with the recently reported crystal structure *Mtb* LpqY bound to trehalose in an open liganded form (the RMSD for 404 superimposed C α atoms is 1.67 Å) (SI Appendix, Fig. S3 B and C) (27). The position and conformation of trehalose are nearly identical in the crystal and cryo-EM structures, except for the O6 hydroxyl group of Glc-1 (Fig. 3). This divergency is caused by the presence of sulfate ions from the crystallization buffer. The Ile251-Ser260 loop of LpqY in the crystal structure has a maximum displacement of around

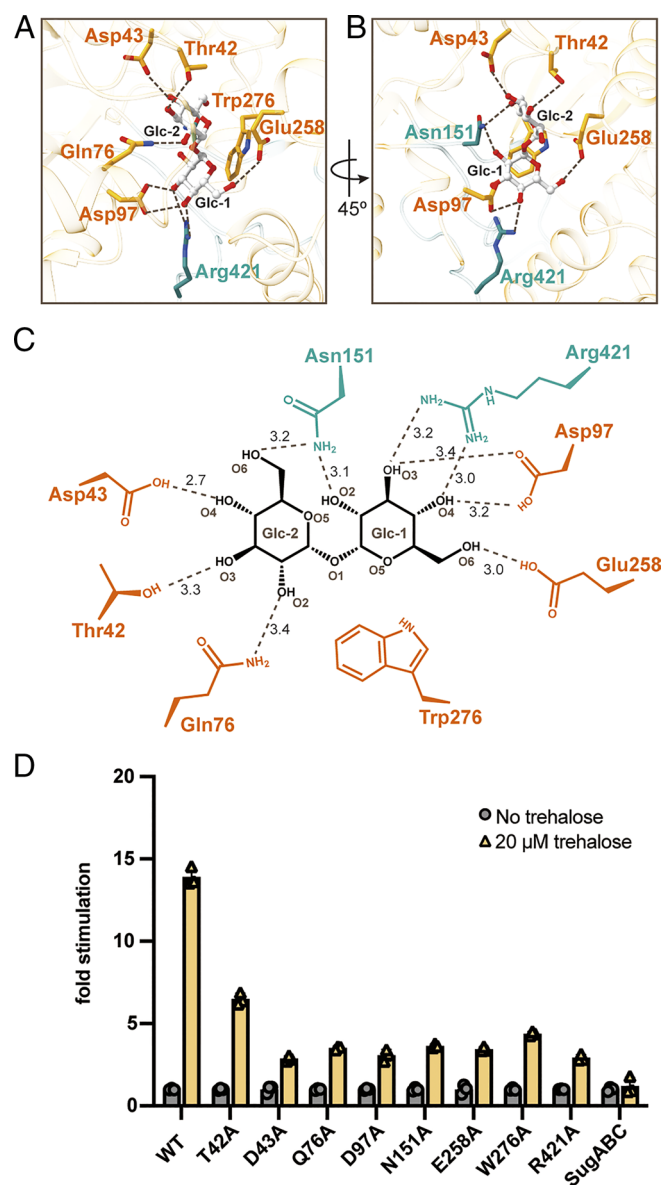
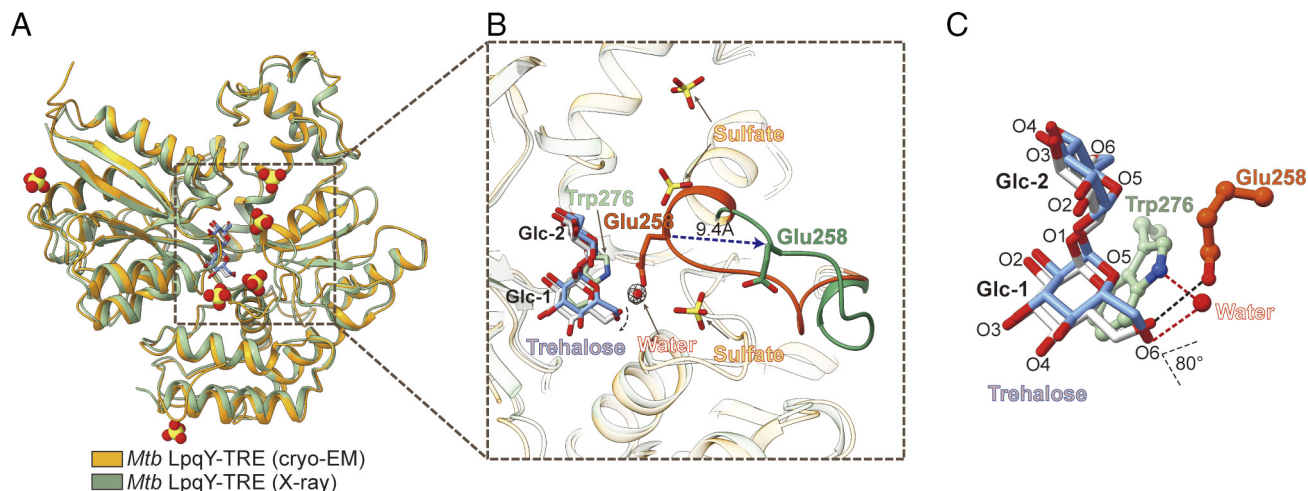


Fig. 2. Trehalose binding site in *Mtb* LpqY. (A and B) Close-up view of the trehalose binding site in *Mtb* LpqY. The residues in the N- and C-lobes of LpqY are colored orange, while the residues in the hinge region are colored teal. Hydrogen bonds are indicated by dashed lines. (C) Schematic diagram of *Mtb* LpqY-trehalose interactions shown in A and B. (D) Trehalose-induced ATPase stimulation of the wild type (WT) and mutant LpqY. SugABC as a negative control. The activity of each protein was normalized to its basal activity without trehalose. Error bars correspond to mean \pm SD (n = 3).



10 Å compared with the cryo-EM structure, while Glu258 involved in coordination with the Glc-1 moiety of trehalose shifts by about 9.4 Å (Fig. 3B). As a result, the hydrogen bond is broken between the O6 hydroxyl group of Glc-1 and the side

chain of Glu258, which makes the O6 hydroxyl group rotate by about 80° (Fig. 3B and C). Instead, the O6 hydroxyl group of Glc-1 makes a new interaction with the side chain of Trp276 mediated by a water molecule in the crystal structure (Fig. 3C).

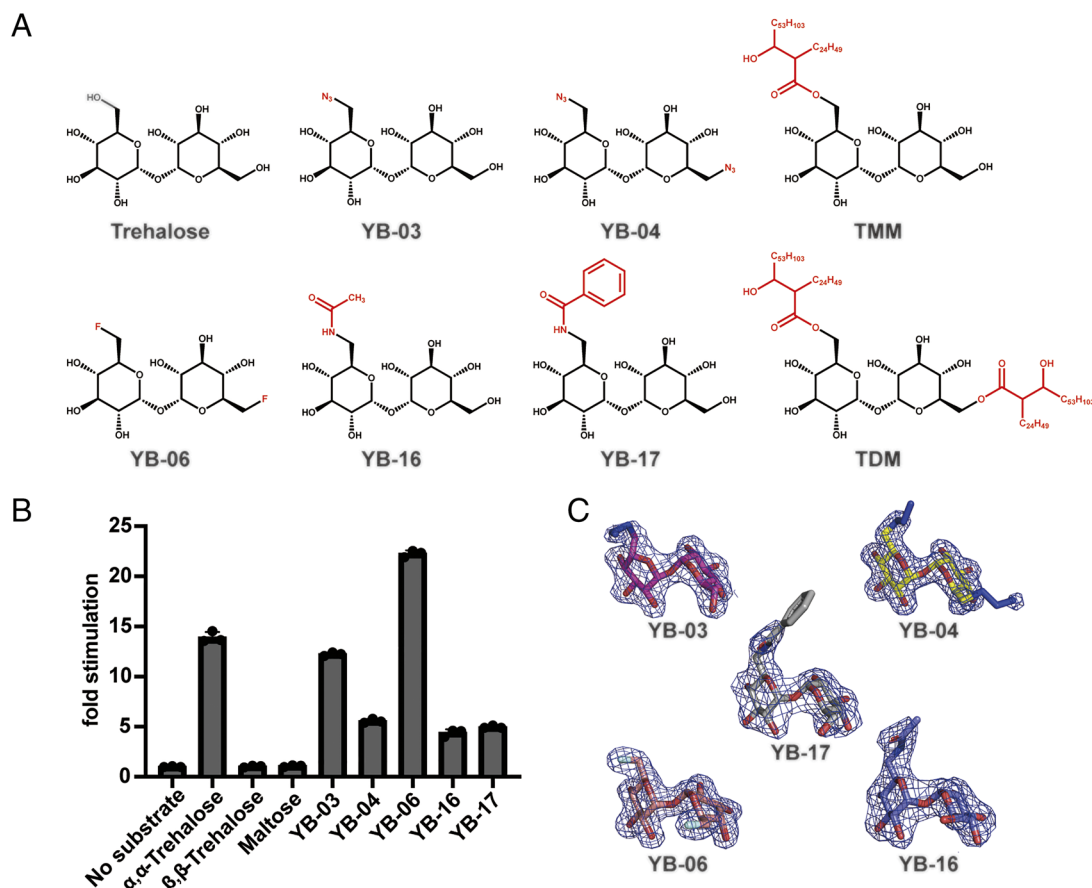


Fig. 4. Trehalose analogues as potential substrates of the trehalose transport system. (A) Trehalose analogues and common trehalose glycolipids. Functional groups distinct from trehalose are highlighted in red. (B) Substrate-induced ATPase stimulation of *Mtb* LpqY-SugABC. The LpqY-SugABC activity for each compound is normalized to the basal activity of LpqY-SugABC without substrate. Error bars correspond to mean \pm SD ($n = 3$). (C) The $2F_o - F_c$ electron densities of trehalose analogues are shown as blue mesh and contoured at 1.0 σ .

A Plastic Substrate Binding Pocket in *Mtb* LpqY. The unexpected presence of sulfate ions near the substrate-binding pocket in the crystal structure of LpqY makes the O6 hydroxyl group of one of the glucose moieties of trehalose have a greater degree of freedom, and also suggests that there is also enough room for larger groups in this location. Intriguingly, the azide-modified trehalose (TreAz) analogue, 6-TreAz, enables interrogation of trehalose in live mycobacteria by metabolic labeling of glycolipids (19). This compound differs from trehalose where an azide group substitutes the O6 hydroxyl group of either glucose moieties (Fig. 4A). Of note, the entry of 6-TreAz into the cytoplasm is the basis for its function, and this process is via the LpqY-SugABC system (19). We synthesized 6-TreAz (YB-03) and performed substrate-stimulated ATPase activity. 6-TreAz significantly promotes the ATPase activity of LpqY-SugABC by approximately 12-fold (Fig. 4B), which is consistent with the ability of this transporter to import it into the cytoplasm. Next, we determined the crystal structure of *Mtb* LpqY in complex with 6-TreAz (Figs. 4C and 5A). As expected, 6-TreAz is firmly locked in the substrate binding pocket of LpqY. Its position and configuration are consistent with trehalose in LpqY, and they interact with the same residues (Fig. 5B and SI Appendix, Fig. S5). Interestingly, the azide group of 6-TreAz is situated on the Glc-1 of trehalose, and toward the interior of LpqY, which is largely identical to the orientation of the O6 hydroxyl group of Glc-1 in trehalose (Fig. 5B). To further investigate whether this location could accommodate larger functional groups, we replaced a hydroxyl group at the 6-position of glucose moiety in trehalose with an acetamide group (6-acetamide-trehalose, YB-16) and a benzamide group (6-benzamide-trehalose, YB-17), respectively (Fig. 4A). ATPase activities showed that these two compounds can still promote the ATPase activity of LpqY-SugABC, but compared

with the physiological substrate, trehalose, the ATPase activity of LpqY-SugABC is drastically decreased (Fig. 4B). Even so, these data also suggest that these two compounds are potential substrates for this transporter. Next, we determined the crystal structures of *Mtb* LpqY in complex with YB-16 and YB-17, respectively. These two compounds are clearly observed in the binding pocket of LpqY, except for the aromatic ring moiety of YB-17 due to its weak density (Fig. 4C and SI Appendix, Fig. S5). Of note, the substituted functional groups are also situated on the Glc-1 of trehalose, but they stretch toward the cleft formed by the N-lobe and C-lobe of LpqY (Fig. 5A and B). Structural analysis showed that the binding modes of these two compounds are nearly identical to that of trehalose, and, in addition, the large substitution groups of YB-16 and YB-17 could generate additional hydrophobic interactions (SI Appendix, Figs. S5 and S6). To investigate why these two compounds induced low ATPase activity of LpqY-SugABC, we superimposed the crystal structures of *Mtb* LpqY and the cryo-EM structure of *Mtb* LpqY-SugABC_{TRE} (Fig. 5E and SI Appendix, Fig. S3D). The results show that the presence of sulfate ions in the crystal structures pushes the Ile251-Ser260 loop of LpqY outward; as a result, this may significantly alter the interaction interface between LpqY and its translocator SugABC in the pretranslocation state (Fig. 5E and SI Appendix, Fig. S3D). Although the crystal structures are nearly identical with the cryo-EM structure in the presence of trehalose, the presence of the sulfate ions in the crystal structures of YB-03 and trehalose appear to contribute to altering the shape and position of the Ile251-Ser260 loop. Interestingly, even in the absence of the sulfate ions in the YB-16- and YB-17-bound structures, in order to accommodate large functional groups, the conformational changes of the Ile251-Ser260 loop are similar to that observed when the sulfate ions are bound. As a

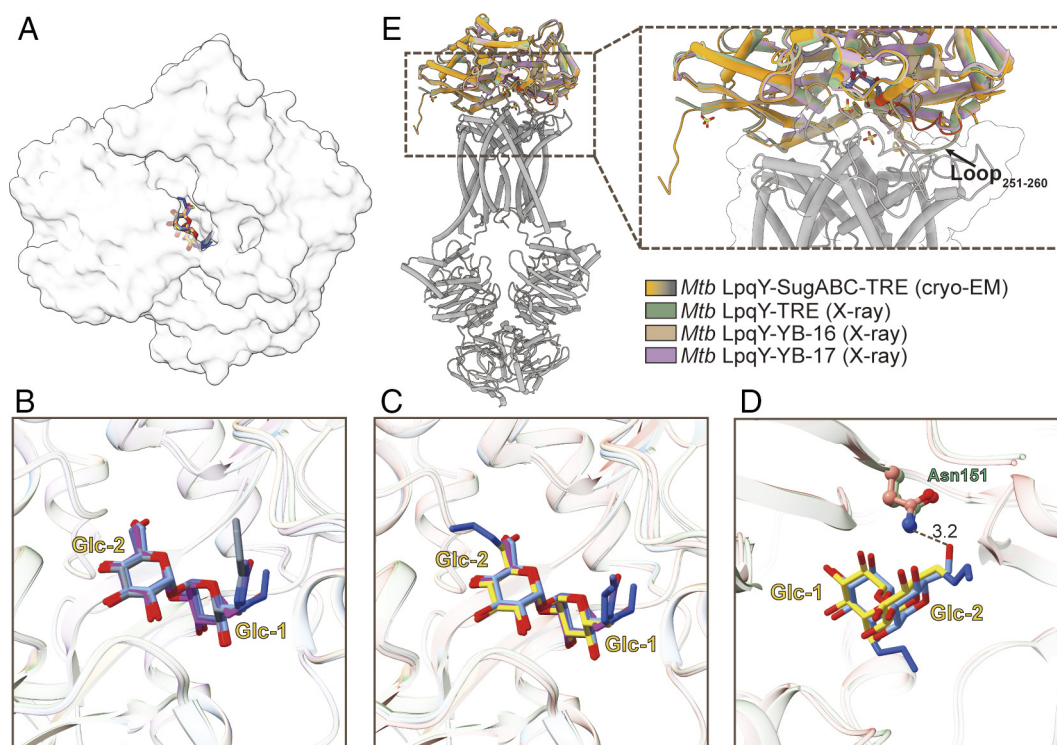


Fig. 5. Structural comparisons of LpqY in complex with trehalose analogues. (A) Surface representation of *Mtb* LpqY with the bound trehalose analogues. *Mtb* LpqY is white and trehalose analogues are shown as stick models. (B) Positions of trehalose (cornflower blue), YB-03 (magenta), YB-16 (slate blue), and YB-17 (slate gray) in the crystal structures. (C) Positions of trehalose (cornflower blue), YB-03 (magenta), YB-04 (yellow) and YB-16 (slate blue) in the crystal structures. (D) Positions of trehalose (cornflower blue) and YB-04 (yellow) in the crystal structures. The hydrogen bond between Asn151 and the O6 hydroxyl group of Glc-2 of trehalose is shown as a dashed line. (E) Superposition of the crystal structures LpqY with three different substrates bound and the cryo-EM structure of LpqY-SugABC in the pretranslocation state. The Ile251-Ser260 loop of LpqY in the cryo-EM structure is highlighted in red.

result, the stability and ATPase activity of LpqY-SugABC will be affected, thus affecting substrate transport. Collectively, these data indicate that certain trehalose analogues might not be able to be transported into cells by the LpqY-SugABC system, despite being recognized and bound by the SBP LpqY. Therefore, it is logical that alternative trehalose derivatives can be designed to block the function of LpqY-SugABC.

The synthesis of many important trehalose-containing glycolipids such as TMM and TDM is initiated at the O6 hydroxyl group of glucose moieties of trehalose in *Mtb* (Fig. 4A) (6). Trehalose derivatives blocking the 6-hydroxyl groups therefore could act as potential inhibitors to disrupt the synthesis of these glycolipids. We further synthesized two trehalose analogues modified at the 6,6'-di- position to investigate whether they could also be recognized by the LpqY-SugABC system. One of the compounds is a fluorine-substituted (6,6'-di-fluoro-trehalose, YB-06), while the other is a compound with a larger azide group (6,6'-di-azido-trehalose, YB-04) (Fig. 4A). The stimulated ATPase activity of LpqY-SugABC by YB-06 is higher than that of the substrate trehalose (Fig. 4B), which is consistent with the chemical properties of fluorine forming a halogen bond that is stronger than the hydrogen bonding that would occur with an oxygen atom (SI Appendix, Fig. S6). YB-04 also showed a substrate-stimulated ATPase activity, but it only increased the ATPase activity of LpqY-SugABC by around 5.5-fold, which is significantly lower than that of YB-03 (Fig. 4B). The co-crystal structures of *Mtb* LpqY bound to these two compounds indicate that these compounds can be recognized by the LpqY-SugABC system, but the presence of the larger azide groups means that YB-04 has a slightly different binding mode compared to trehalose (Fig. 5 C and D). The density for the azide group of Glc-2 in YB-04 is weak (Fig. 4C), which may be due to the loss of a hydrogen bond to Asn151 (Fig. 5D and SI Appendix, Fig. S5). As a result, the orientation of the azide group of Glc-2 in YB-04 is different from that of the hydroxyl group of trehalose at the same position (Fig. 5C). In addition, the orientation of the azide group of Glc-1 in YB-04 is similar to the acetamide group of YB-16, but different compared with the azide group of YB-03 (Fig. 5C). Therefore, YB-04 has a low induced stimulation of ATPase activity. Collectively, these results suggest that the trehalose binding protein LpqY possesses a plastic substrate binding pocket, a feature that can facilitate the design of diverse trehalose derivatives for the application of molecular probes or as enzyme inhibitors.

Conclusion

The trehalose-rich glycolipids are essential for the survival and pathogenicity of *Mtb*. Disrupting the synthesis of these glycolipids is therefore a promising direction for the development of new anti-TB drugs. The presence of a trehalose metabolism pathway in mycobacteria suggests that trehalose analogues can serve as inhibitors of the LpqY-SugABC complex or other enzymes or become incorporated into the mycomembrane. Importantly, the LpqY-SugABC system acts as the critical trehalose transport pathway, which can allow trehalose analogues to enter the cytoplasm. Our structural and functional results have revealed how LpqY recognizes and binds trehalose and its analogues in this system. In addition, we have characterized a plastic substrate binding pocket in LpqY, which can facilitate rational structure-based trehalose derivative design. Furthermore, the establishment of substrate-stimulated ATPase activity of LpqY-SugABC will help to screen ligands that target this system. Our data therefore lay a vital foundation for the application of trehalose analogues in the field of tuberculosis as potential molecular probe tools or as anti-TB drugs.

Materials and Methods

Expression and Purification of *Mtb* LpqY-SugABC. The genes encoding full-length LpqY-SugABC (Rv1235-Rv1238) were cloned from *Mtb* strain H37Rv genomic DNA and inserted into a pMV261 vector, fused with a C-terminal 10× His tag attached to SugC. All mutations were generated using the Fast Mutagenesis System (TransGen). The recombinant plasmids were transformed into *M. smegmatis* mc²155 cells for expression. The cells were cultivated at 37 °C in Luria broth (LB) liquid media supplemented with 50 µg mL⁻¹ kanamycin, 20 µg mL⁻¹ carbenicillin, and 1 g L⁻¹ Tween80 until the optical density (OD₆₀₀) reached 1.0. Overexpression of the proteins was induced by 0.2% (w/v) acetamide at 16 °C for 4 d. Harvested cells pellets were resuspended in buffer A containing 20 mM HEPES pH 7.5, 150 mM NaCl, lysed by passing through a high-pressure homogenizer at 1,200 bars, and centrifuged at 12,000 rpm for 10 min at 4 °C to removed cell debris. The supernatant was collected and ultracentrifuged at 37,000 rpm for 1.5 h to isolate the membrane fractions. The membrane fraction was resuspended in buffer A supplemented with 1 mM trehalose. After incubating with 1% (w/v) lauryl maltose neopentyl glycol (LMNG; Anatrace) for 1.5 h at 4 °C, the suspension was centrifuged and the supernatant supplemented with 20 mM imidazole was loaded onto a Ni-NTA agarose beads (QIAGEN) affinity column. The beads were then washed in buffer A supplemented with 50 mM imidazole and 0.005% (w/v) LMNG, and then exchanged into 0.04% (w/v) GDN buffer. The protein was eluted from the beads with buffer A supplemented with 500 mM imidazole, 0.04% (w/v) GDN, 1 mM trehalose and 10 mM DTT, and then concentrated and loaded to a size-exclusion chromatography column (Superose 6 Increase 10/300 GL, GE Healthcare) preequilibrated with 20 mM HEPES pH 7.5, 150 mM NaCl, 2 mM trehalose, 2 mM DTT and 0.04% (w/v) GDN. The peak fractions were pooled and concentrated for cryo-EM sample preparation using a 100-kDa cutoff concentrator (Merck Millipore). All mutants were overexpressed using the same protocol as the wild-type protein and purified with the detergent LMNG. Finally, they were stored in buffer containing 20 mM HEPES pH 7.5, 150 mM NaCl, 2 mM DTT, 5 mM MgCl₂ and 0.005% (w/v) LMNG.

Expression and Purification of *Mtb* LpqY. The DNA sequence encoding full-length LpqY (residues 1-468aa) was amplified from *Mtb* strain H37Rv genomic by PCR and then inserted into the pET-22b (+) vector with a C-terminal 6×His tag. The recombinant plasmid was transformed into the *E. coli* strain of BL21(DE3) cells. Cells were cultivated in Luria broth (LB) liquid media supplemented 50 µg mL⁻¹ ampicillin at 37 °C until the optical density (OD₆₀₀) reached 0.6 to 0.8. Overexpression of protein was induced by 200 µM isopropyl-b-D-thiogalactoside (IPTG) at 16 °C for 16 h. For purification, harvested cells were resuspended in buffer A supplemented with 1 mM phenylmethylsulfonyl fluoride (PMSF) and lysed by passing through a high-pressure homogenizer at 800 bar. Cells debris was removed by centrifugation at 18,000 rpm for 40 min at 4 °C, and then, the supernatant was loaded onto a Ni-NTA agarose beads (QIAGEN) affinity column for 2 h. The beads were then washed in buffer A supplemented with 50 mM imidazole. The protein was then eluted from the beads with buffer A supplemented with 500 mM imidazole. The elution sample was further purified by ion-exchange chromatography (HiTrap™ Q HP, GE Healthcare) and size exclusion chromatography (Superdex 200 GE Healthcare). The peak fractions were concentrated to 8 to 10 mg mL⁻¹ and stored for crystallization.

Electron Microscopy Sample Preparation and Data Collection. First, 3 µL of purified *Mtb* LpqY-SugABC sample at 4 mg mL⁻¹ was loaded onto a freshly glow-discharged holey carbon grid (Quantifoil Cu R1.2/1.3). Grids were then blotted for 2.5 s and flash-frozen in liquid ethane cooled by liquid nitrogen using an FEI Mark IV Vitrobot (FEI) operated at 8 °C and 100% humidity. Cryo-EM data were collected on an FEI Titan Krios electron microscope operated at 300 keV with a Gatan K3 camera at 29,000× nominal magnification in superresolution mode and binned to a pixel size of 0.832 Å/pixel. All data were collected with a defocus range from -1.2 to -2.0 µm. Automated single-particle data acquisition was performed with SerialEM (32).

Electron Microscopy Data Analysis. Alignment and motion correction were performed using MotionCorr2 (33), with a five-by-four patch-based alignment. Subsequent steps were performed using cryoSPARC (34). A total of 3,561 micrographs were recorded and aligned. Micrographs that exhibited defects in the Thon rings due to excessive drift, ice contamination, or astigmatism were discarded.

A total 1,442,141 particles of LpqY-SugABC were automatically selected, extracted from micrographs with a box size of 384 pixels, and submitted for several rounds of reference-free 2D classification to discard bad particles. After particle cleaning, 119,568 particles were used for ab initio reconstruction to generate 3D models as references to perform heterogeneous refinement. After heterogeneous refinement, the best group with 50,775 particles was refined using Homogeneous Refinement and NU-Refinement to generate the final cryo-EM map with an estimated average resolution of 3.02 Å based on the gold-standard Fourier shell correlation cutoff of 0.143 (35). Local resolution ranges were also analyzed within cryoSPARC.

Model Building. Model building of *Mtb* LpqY-SugABC in complex with trehalose was based on 3.02 Å cryo-EM map and the cryo-EM structure of *M. smegmatis* LpqY-SugABC in the pretranslocation state (PDB ID: 7CAF). This model was docked into the cryo-EM map using UCSF Chimera (36) and manually adjusted using Coot (37). Several iterations of real-space refinement were performed in PHENIX (38). The final atomic model was evaluated using MolProbity (39). Cryo-EM data collection and model refinement statistics are shown in [SI Appendix, Table S1](#). All structural figures were prepared using UCSF ChimeraX (40) or PyMol (www.pymol.org).

ATPase Activity Assay. The ATPase activity of *Mtb* LpqY-SugABC and mutants were measured using a modified version of the malachite green assay (41). LpqY-SugABC or the mutant sample was diluted to 0.28 to 0.35 μM in reaction buffer (20 mM HEPES pH 7.5, 150 mM NaCl, 0.005% (w/v) LMNG, 1 mM DTT, 5 mM MgCl₂ and 4 mM ATP) and incubated at 37 °C for 5 min. The substrates-stimulated ATPase activities of LpqY-SugABC and mutants were determined using the same protocol. Trehalose or trehalose analogs were extra added to reaction buffer at a final concentration of 20 μM. The reaction was stopped and colored with the reagent [3:1 mixture of 0.05% malachite green and 4.2% (w/v) ammonium molybdate in 4 N HCl, 0.06% (w/v) Tween 20]. After 1 min, 24% (w/v) sodium citrate was added to prevent further coloring caused by newly release of phosphate. The quenched reactions were incubated at room temperature for 30 min. The amount of produced phosphate was detected by absorbance at 660 nm measured on a Molecular Devices ID3 reader. The experiments were performed at least three times. Results were analyzed in GraphPad Prism 9.0 (<https://www.graphpad.com>).

Crystallization, Data Collection, and Structure Determination. *Mtb* LpqY was incubated with 2 mM trehalose for 1 h at 4 °C, and the complex (8 mg mL⁻¹) was crystallized by the sitting drop vapor diffusion method at 20 °C. The best crystals were grown with well buffer containing 50 mM magnesium sulfate hydrate, 50 mM HEPES sodium pH 7.0, and 1.6 M lithium sulfate monohydrate. Analogue-bound crystals were obtained in the same condition by co-crystallization in the presence of 2 mM trehalose analogs. Crystals were harvested using 20% (v/v) glycerol as cryoprotectant, flash-cooled, and stored in liquid nitrogen for data collection.

X-ray data were collected on beamlines BL17U1 and BL19U1 at the Shanghai Synchrotron Radiation Facility and BL41XU at Spring 8. Data integration and scaling were performed using the program XDS (42). The structures were determined by molecular replacement (MR) with the cryo-EM structure LpqY-bound trehalose as a search model using the program PHASER (43). The output model from MR

was subsequently subjected to iterative cycles of manual model adjustment with Coot, and refinement was completed using Phenix (38). Trehalose and trehalose analogues were built based on the omit maps. Data collection and structure refinement statistics are summarized in [SI Appendix, Table S2](#).

Microscale Thermophoresis (MST) Assay. Binding affinities of trehalose and trehalose analogues with *Mtb* LpqY were measured using the MST assay method. MST measurements were conducted on the Monolith NT.Automated (Nanotemper Technologies) with 20% LED power and medium MST power. The proteins were fluorescently labeled according to the manufacturer's procedure and kept in the MST buffer (20 mM HEPES pH 7.5, 300 mM NaCl) at a concentration of 200 nM and incubated for 30 min at 25 °C in the dark. For each assay, the labeled protein was mixed with the same volume of unlabeled compound at 12 different serially diluted concentrations at room temperature. Each assay was repeated three times. Data analyses were performed using MO. Affinity Analysis v.2.2.4 software. There is 95% confidence that the *K_d* value is within the given range. Figures were made by GraphPad Prism 9.0.

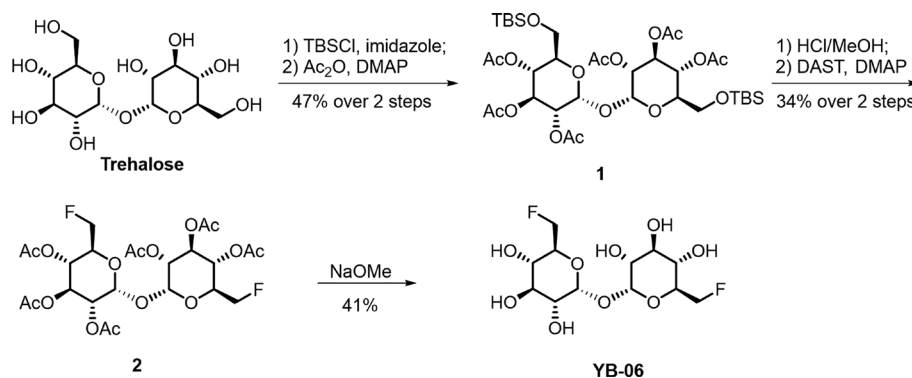
Chemical Synthesis of Trehalose Analogue. Trehalose (3.42 g, 10.0 mmol) was dissolved in dry DMF (10 mL), warmed to 50 °C. Then, imidazole (1.36 g, 20.0 mmol) and TBSCl (2.27 g, 15.0 mmol) were added at room temperature. The reaction mixture was stirred for another 1 h at room temperature. The mixture was evaporated in vacuo. The residue was redissolved in dry pyridine (100 mL); then, DMAP (122 mg, 1 mmol) was added, cooled to 0 °C, and Ac₂O (7.52 mL, 80.0 mmol) was added dropwise during 10 min. Then, the ice bath was removed, and the reaction mixture was stirred for another 8 h at room temperature. The mixture was evaporated in vacuo, and the residue was purified by column chromatography using silica gel (Petroleum ether/EtOAc, 6:1 v/v) to afford compound **1** (3.94 g, 47%) as a white foam.

¹H NMR (500 MHz, CDCl₃) δ = 5.47 (t, *J* = 9.8, 2H), 5.24 (d, *J* = 3.9, 2H), 5.11–4.98 (m, 4H), 3.92 (d, *J* = 10.2, 2H), 3.68–3.57 (m, 4H), 2.08 (s, 6H), 2.03 (t, *J* = 6.4, 12H), 0.86 (s, 18H), 0.04–0.00 (m, 12H).

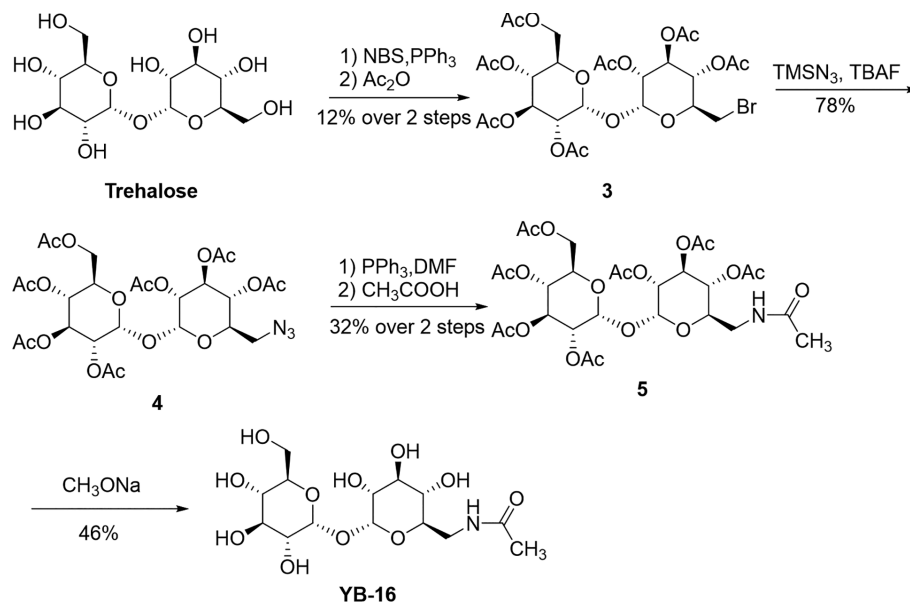
Compound **1** (824 mg, 1.0 mmol) was dissolved in HCl (0.13 mol/L) and stirred for 0.5 h at 0 °C. The mixture was evaporated in vacuo, the residue was redissolved in DCM and washed with saturated NaHCO₃ aqueous solution (3 × 50 mL). The organic layer was concentrated in vacuo, and the residue was used for next step directly without further purification. The residue above and DMAP (256 mg, 2.1 mmol) was dissolved in dry DCM (100 mL) and cooled to 0 °C. Then, DAST (322 mg, 2.0 mmol) was added dropwise at 0 °C; the ice bath was removed and the reaction mixture stirred at ambient temperature for 2 h. The reaction mixture was poured into ice, stayed still and separated, and extracted with DCM, and the organic layer was washed with saturated NaHCO₃ aqueous solution (3 × 50 mL). The organic layer was evaporated in vacuo, and the residue was purified by column chromatography (EtOAc) to afford compound **2** as a light yellow foam (204 mg, 34%).

¹H NMR (400 MHz, CDCl₃) δ = 5.51 (t, *J* = 9.8, 2H), 5.31–5.28 (m, 2H), 5.08–5.00 (m, 4H), 4.47 (dd, *J* = 6.0, 4.0, 2H), 4.38–4.32 (m, 2H), 4.19 (m, 2H), 2.14–1.99 (m, 18H).

Compound **2** (19 mg, 0.15 mmol) was dissolved in dry methanol (2 mL). Then, MeONa (1 mg, 0.18 mmol) was added. The reaction mixture was stirred at ambient temperature for 20 min. Then, acid resin was added to adjust pH



Scheme 1. Synthesis of YB-06.



Scheme 2. Synthesis of YB-16.

to 7 to 8. The mixture was filtered, and the filtrate concentrated and purified by C18 reverse phase column chromatography (MeOH/H₂O, 8:1 v/v) to afford compound **3** (YB-06) (4.5 mg, 41%) as a colorless oil. ¹H NMR (600 MHz, CD₃OD) δ 5.06 (d, *J* = 3.7 Hz, 2H), 4.65 (dd, *J* = 10.2, 3.8 Hz, 1H), 4.61–4.54 (m, 2H), 4.50 (dd, *J* = 10.2, 1.6 Hz, 1H), 4.04–3.91 (m, 2H), 3.78 (t, *J* = 9.3 Hz, 2H), 3.46 (dd, *J* = 9.8, 3.7 Hz, 2H), 3.38 (dd, *J* = 10.1, 9.1 Hz, 2H). ¹³C NMR (150 MHz, CD₃OD) δ 94.2, 82.3, 81.2, 73.1, 71.6, 71.3, 69.3. HR-MS (ESI-TOF): *m/z* [M+Na]⁺ calcd for C₁₂H₂₀F₂O₉Na⁺ 369.0968, found 369.0971 (Scheme 1).

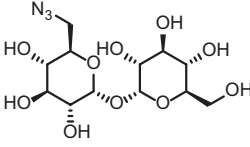
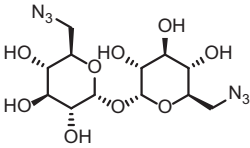
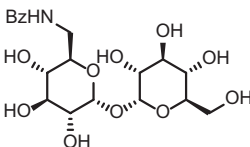
Trehalose (10.0 g, 29.2 mmol) and PPh₃ (15.3 g, 58.4 mmol) were dissolved in dry DMF (500 mL). Then, NBS (6.76 g, 38.0 mmol) was added at 0 °C. The reaction mixture was warmed to 80 °C and stirred for another 8 h. The reaction solution was cooled to room temperature and concentrated. The residue was purified by rapid column chromatography (DCM/MeOH, 5:1 v/v) to obtain 2.2 g brown crude product. The brown solid above (2.2 g, 5.44 mmol) was dissolved in dry pyridine (50 mL); acetic anhydride (5.1 mL, 54.4 mmol) was added dropwise. The reaction mixture was stirred overnight at room temperature. The mixture was evaporated in vacuo, and the residue was purified by column chromatography (Petroleum ether/EtOAc, 4:1 v/v) to afford compound **3** (12.4 g, 12% over two steps) as a white foam. ¹H NMR (400 MHz, CDCl₃) δ 5.48 (dd, *J* = 18.3, 9.3 Hz, 2H), 5.32 (t, *J* = 3.5 Hz, 2H), 5.14 (dd, *J* = 10.3, 3.9 Hz, 1H), 5.01 (ddd, *J* = 32.2, 14.8, 8.1 Hz, 3H), 4.22 (dd, *J* = 12.3, 5.9 Hz, 1H), 4.16–3.96 (m, 3H), 3.34 (ddd, *J* = 18.9, 11.2, 5.1 Hz, 2H), 2.15–1.99 (m, 21H); ESI-LRMS (*m/z*) 721.30 [M+Na]⁺.

Compound **3** (1.0 g, 1.43 mmol) was dissolved in dry DMF (300 mL), then TMSN₃ (0.283 mL, 215 mmol) and 1 M TBAF in THF (2.15 mL, 2.15 mmol) were added, warmed to 50 °C and stirred for 8 h. The mixture was evaporated in vacuo, and the residue was purified by column chromatography (petroleum ether/EtOAc, 4:1 v/v) to afford compound **4** (738 mg, 78%) as a white foam. ¹H NMR (400 MHz, CDCl₃) δ = 5.48 (td, *J* = 9.8, 5.8, 2H), 5.31 (dd, *J* = 8.1, 3.5, 2H), 5.13–4.93 (m, 4H), 4.25 (dd, *J* = 12.2, 5.6, 1H), 4.12–3.94 (m, 3H), 3.34 (d, *J* = 7.3, 1H), 3.21–3.10 (m, 1H), 2.15–1.99 (m, 21H); ESI-LRMS (*m/z*) 684.25 [M+Na]⁺.

Compound **4** (200 mg, 0.303 mmol) was dissolved in dry DMF (300 mL). PPh₃ (397 mg, 1.52 mmol) was added and stirred at room temperature overnight. Then, Ac₂O (87 μL, 1.52 mmol) was added dropwise and allowed to react overnight at room temperature. The mixture was evaporated in vacuo, and the residue was purified by column chromatography (Petroleum ether/EtOAc, 6:1 v/v) to afford compound **5** (365 mg, 32% over 2 steps) as a white foam. ¹H NMR (400 MHz, CDCl₃) δ = 5.86 (s, 1H), 5.45 (td, *J* = 9.8, 4.4, 2H), 5.28 (dd, *J* = 28.6, 3.8, 2H), 5.09–4.70 (m, 4H), 4.30–3.92 (m, 4H), 3.81 (dd, *J* = 8.7, 6.1, 1H), 3.52 (d, *J* = 6.4, 1H), 3.34–3.10 (m, 1H), 2.05 (s, 12H), 2.02 (s, 3H), 2.00 (d, *J* = 2.8, 6H), 1.97 (s, 3H); ESI-LRMS (*m/z*) 700.13 [M+Na]⁺.

Compound **5** (30 mg, 0.0443 mmol) was dissolved in dry methanol (1.5 mL) and CH₂Cl₂ (1.5 mL). Then, MeONa (1 mg, 0.18 mmol) was added and allowed to react overnight at room temperature. The solvents were evaporated in vacuo, and the residue purified by column chromatography using silica gel (DCM/MeOH, 5:1 v/v) to afford compound **YB-16** (8 mg, 46%) as a white foam. ¹H NMR (400 MHz, D₂O) δ = 5.17 (t, *J* = 4.1, 2H), 3.98–3.73 (m, 6H), 3.73–3.54 (m, 3H), 3.53–3.40 (m, 2H), 3.4–3.32 (m, 1H), 2.03 (s, 3H); HR-MS (ESI-TOF): *m/z* [M+Na]⁺ calcd for C₁₄H₂₅NO₁₁ [M+Na]⁺ 406.1320, found 406.1316 (Scheme 2).

The known compounds:

1	YB-03		(44)
2	YB-04		(45)
3	YB-17		(46)

Data, Materials, and Software Availability. All data are available in the manuscript. The accession number for the 3D cryo-EM density map of *Mtb* LpqY-SugABC with Trehalose bound is [EMD-36125](#) (47). Atomic coordinates and structure factors for the *Mtb* LpqY-SugABC_{TRE}, LpqY-TRE, LpqY-YB-03, LpqY-YB-04, LpqY-YB-06, LpqY-YB-16, and LpqY-YB-17 structures have been deposited in the Protein Data Bank (PDB) with identification codes [8JA7](#) (48), [8JAB](#) (49), [8JA9](#) (50), [8JAA](#) (51), [8JAB](#) (52), [8JAC](#) (53), and [8JAD](#) (54).

ACKNOWLEDGMENTS. We thank the staff from the Electron Microscopy Facility of ShanghaiTech University and the beamlines BL19U1, BL17U1 and BL17UM of Shanghai Synchrotron Radiation Facility, and BL41XU at Spring 8, for assistance during data collection. We are thankful to the Analytical chemistry platform of

Shanghai Institute for Advanced Immunochemical Studies. This work was supported by grants from the National Natural Science Foundation of China (Grant Nos. 32171217 to B.Z. and 32200983 to F.L.), Shanghai Sailing Program (Grant No. 21YF1429700 to B.Z.), Young Elite Scientists Sponsorship Program by CAST (Grant No. 2021QNRC001 to B.Z.), Shanghai Municipal Science and Technology Major Project, and the Shanghai Frontiers Science Center for Biomacromolecules and Precision Medicine, ShanghaiTech University.

Author affiliations: ^aState Key Laboratory of Medicinal Chemical Biology, Nankai University, Tianjin 300353, China; ^bShanghai Institute for Advanced Immunochemical Studies and School of Life Science and Technology, ShanghaiTech University, Shanghai 201210, China; ^cInnovative Center For Pathogen Research, Guangzhou Laboratory, Guangzhou 510005, China; ^dState Key Laboratory of Bioorganic and Natural Products Chemistry, Shanghai Institute of Organic Chemistry, Chinese Academy of Sciences, Shanghai 200032, China; ^eLaboratory of Structural Biology, Tsinghua University, Beijing 100084, China; ^fShanghai Clinical Research and Trial Center, Shanghai 201210, China; and ^gSchool of Chemistry and Molecular Biosciences, The University of Queensland, Brisbane, QLD 4072, Australia

- WHO, Global Tuberculosis Report 2020 (2020).
- S. Gagneux, Host-pathogen coevolution in human tuberculosis. *Philos. Trans. R Soc. Lond. B Biol. Sci.* **367**, 850–859 (2012).
- S. Ehart, D. Schnappinger, K. Y. Rhee, Metabolic principles of persistence and pathogenicity in *Mycobacterium tuberculosis*. *Nat. Rev. Microbiol.* **16**, 496–507 (2018).
- E. J. North, M. Jackson, R. E. Lee, New approaches to target the mycolic acid biosynthesis pathway for the development of tuberculosis therapeutics. *Curr. Pharm. Des.* **20**, 4357–4378 (2014).
- Z. S. Bhat *et al.*, Cell wall: A versatile fountain of drug targets in *Mycobacterium tuberculosis*. *Biomed. Pharmacother.* **95**, 1520–1534 (2017).
- A. Nobre, S. Alarico, A. Maranha, V. Mendes, N. Empadinhas, The molecular biology of mycobacterial trehalose in the quest for advanced tuberculosis therapies. *Microbiology* **160**, 1547–1570 (2014).
- E. Ishikawa *et al.*, Direct recognition of the mycobacterial glycolipid, trehalose dimycolate, by C-type lectin Mincle. *J. Exp. Med.* **206**, 2879–2888 (2009).
- H. Yamagami *et al.*, Trehalose 6,6'-dimycolate (cord factor) of *Mycobacterium tuberculosis* induces foreign-body- and hypersensitivity-type granulomas in mice. *Infect. Immun.* **69**, 810–815 (2001).
- H. Marrakchi, M. A. Laneelle, M. Daffe, Mycolic acids: Structures, biosynthesis, and beyond. *Chem. Biol.* **21**, 67–85 (2014).
- R. Kalscheuer, B. Weinrick, U. Veeraraghavan, G. S. Besra, W. R. Jacobs Jr., Trehalose-recycling ABC transporter LpqY-SugA-SugB-SugC is essential for virulence of *Mycobacterium tuberculosis*. *Proc. Natl. Acad. Sci. U.S.A.* **107**, 21761–21766 (2010).
- J. M. Wolber *et al.*, The trehalose-specific transporter LpqY-SugABC is required for antimicrobial and anti-biofilm activity of trehalose analogues in *Mycobacterium smegmatis*. *Carbohydr. Res.* **450**, 60–66 (2017).
- S. H. Liyanage *et al.*, Azide-masked fluorescence turn-on probe for imaging mycobacteria. *JACS Au*, **3**, 1017–1028 (2023).
- Z. Xu, V. A. Meshcheryakov, G. Poce, S. S. Chng, MmpL3 is the flippase for mycolic acids in mycobacteria. *Proc. Natl. Acad. Sci. U.S.A.* **114**, 7993–7998 (2017).
- B. Zhang *et al.*, Crystal structures of membrane transporter MmpL3, an anti-TB drug target. *Cell* **176**, 636–648.e13 (2019).
- N. Sathyanmoorthy, K. Takayama, Purification and characterization of a novel mycolic acid exchange enzyme from *Mycobacterium smegmatis*. *J. Biol. Chem.* **262**, 13417–13423 (1987).
- J. T. Belisle *et al.*, Role of the major antigen of *Mycobacterium tuberculosis* in cell wall biogenesis. *Science* **276**, 1420 (1997).
- A. A. Pohane, C. R. Carr, J. Garhyhan, B. M. Swarts, M. S. Siegrist, Trehalose recycling promotes energy-efficient biosynthesis of the Mycobacterial cell envelope. *mBio* **12**, e02801-20 (2021).
- K. M. Backus *et al.*, Uptake of unnatural trehalose analogs as a reporter for *Mycobacterium tuberculosis*. *Nat. Chem. Biol.* **7**, 228–235 (2011).
- B. M. Swarts *et al.*, Probing the mycobacterial trehalome with bioorthogonal chemistry. *J. Am. Chem. Soc.* **134**, 16123–16126 (2012).
- F. P. Rodriguez-Rivera, X. Zhou, J. A. Theriot, C. R. Bertozzi, Visualization of mycobacterial membrane dynamics in live cells. *J. Am. Chem. Soc.* **139**, 3488–3495 (2017).
- T. Dai *et al.*, A fluorogenic trehalose probe for tracking phagocytosed *Mycobacterium tuberculosis*. *J. Am. Chem. Soc.* **142**, 15259–15264 (2020).
- M. Kamariza *et al.*, Rapid detection of *Mycobacterium tuberculosis* in sputum with a solvatochromic trehalose probe. *Sci. Transl. Med.* **10**, eaam6310 (2018).
- H. A. Sahile, C. Rens, T. Shapira, R. J. Andersen, Y. Av-Gay, DMN-Tre labeling for detection and high-content screening of compounds against intracellular Mycobacteria. *ACS Omega* **5**, 3661–3669 (2020).
- R. P. A. Berntsson, S. H. J. Smits, L. Schmitt, D. J. Slotboom, B. Poolman, A structural classification of substrate-binding proteins (vol 584, pg 2606, 2010). *FEBS Lett.* **584**, 4373–4373 (2010).
- M. Rezwan, T. Grau, A. Tschumi, P. Sander, Lipoprotein synthesis in mycobacteria. *Microbiology* **153**, 652–658 (2007).
- F. Liu *et al.*, Structural basis of trehalose recycling by the ABC transporter LpqY-SugABC. *Sci. Adv.* **6**, eabb9833 (2020).
- D. Sharma, M. Singh, P. Kaur, U. Das, Structural analysis of LpqY, a substrate-binding protein from the SugABC transporter of *Mycobacterium tuberculosis*, provides insights into its trehalose specificity. *Acta Crystallogr. D Struct. Biol.* **78**, 835–845 (2022).
- L. Bishop, R. Agbayani Jr., S. V. Ambudkar, P. C. Maloney, G. F. Ames, Reconstitution of a bacterial periplasmic permease in proteoliposomes and demonstration of ATP hydrolysis concomitant with transport. *Proc. Natl. Acad. Sci. U.S.A.* **86**, 6953–6957 (1989).
- M. L. Mimmack *et al.*, Energy coupling to periplasmic binding protein-dependent transport systems: Stoichiometry of ATP hydrolysis during transport in vivo. *Proc. Natl. Acad. Sci. U.S.A.* **86**, 8257–8261 (1989).
- J. Chen, Molecular mechanism of the *Escherichia coli* maltose transporter. *Curr. Opin. Struct. Biol.* **23**, 492–498 (2013).
- D. Khare, M. L. Oldham, C. Orelle, A. L. Davidson, J. Chen, Alternating access in maltose transporter mediated by rigid-body rotations. *Mol. Cell* **33**, 528–536 (2009).
- D. N. Mastronarde, Automated electron microscope tomography using robust prediction of specimen movements. *J. Struct. Biol.* **152**, 36–51 (2005).
- S. Q. Zheng *et al.*, MotionCor2: Anisotropic correction of beam-induced motion for improved cryo-electron microscopy. *Nat. Methods* **14**, 331–332 (2017).
- A. Punjani, J. L. Rubinstein, D. J. Fleet, M. A. Brubaker, cryoSPARC: Algorithms for rapid unsupervised cryo-EM structure determination. *Nat. Methods* **14**, 290–296 (2017).
- N. Grigorieff, FREALIGN: An exploratory tool for single-particle cryo-EM. *Methods Enzymol.* **579**, 191–226 (2016).
- E. F. Pettersen *et al.*, UCSF Chimera-A visualization system for exploratory research and analysis. *J. Comput. Chem.* **25**, 1605–1612 (2004).
- P. Emsley, B. Lohkamp, W. G. Scott, K. Cowtan, Features and development of Coot. *Acta Crystallogr. D Biol. Crystallogr.* **66**, 486–501 (2010).
- P. V. Afonine *et al.*, Joint X-ray and neutron refinement with phenix.refine. *Acta Crystallogr. D Biol. Crystallogr.* **66**, 1153–1163 (2010).
- V. B. Chen *et al.*, MolProbity: All-atom structure validation for macromolecular crystallography. *Acta Crystallogr. D Biol. Crystallogr.* **66**, 12–21 (2010).
- T. D. Goddard *et al.*, UCSF ChimeraX: Meeting modern challenges in visualization and analysis. *Protein Sci.* **27**, 14–25 (2018).
- P. A. Lanzetta, L. J. Alvarez, P. S. Reinach, O. A. Candia, An improved assay for nanomole amounts of inorganic phosphate. *Anal. Biochem.* **100**, 95–97 (1979).
- W. Kabsch, Xds. *Acta Crystallogr. D Biol. Crystallogr.* **66**, 125–132 (2010).
- A. J. McCoy *et al.*, Phaser crystallographic software. *J. Appl. Crystallogr.* **40**, 658–674 (2007).
- M. Wang, P. F. Tu, Z. D. Xu, X. L. Yu, M. Yang, Design and synthesis of guanidinoglycosides directed against the TAR RNA of HIV-1. *Helv. Chim. Acta* **86**, 2637–2644 (2003).
- F. M. Menger, B. N. Mbadugha, Gemini surfactants with a disaccharide spacer. *J. Am. Chem. Soc.* **123**, 875–885 (2001).
- J. D. Rose *et al.*, Synthesis and biological evaluation of trehalose analogs as potential inhibitors of mycobacterial cell wall biosynthesis. *Carbohydr. Res.* **337**, 105–120 (2002).
- J. X. Liang, Z. H. Rao, B. Zhang, Cryo-EM structure of *Mycobacterium tuberculosis* LpqY-SugABC in complex with trehalose. Electron Microscopy Data Bank. <https://www.ebi.ac.uk/emdb/EMD-36125>. Deposited 5 May 2023.
- B. Zhang, J. X. Liang, Z. H. Rao, Cryo-EM structure of *Mycobacterium tuberculosis* LpqY-SugABC in complex with trehalose. RCSB Protein Data Bank. <https://www.rcsb.org/structure/unreleased/8JA7>. Deposited 5 May 2023.
- B. Zhang, J. X. Liang, Z. H. Rao, Crystal structure of *Mycobacterium tuberculosis* LpqY with trehalose bound in a closed liganded form. RCSB Protein Data Bank. <https://www.rcsb.org/structure/unreleased/8JA8>. Deposited 5 May 2023.
- B. Zhang, J. X. Liang, Z. H. Rao, Crystal structure of *Mycobacterium tuberculosis* LpqY in complex with trehalose analogue YB-03. RCSB Protein Data Bank. <https://www.rcsb.org/structure/unreleased/8JA9>. Deposited 5 May 2023.
- B. Zhang, J. X. Liang, Z. H. Rao, Crystal structure of *Mycobacterium tuberculosis* LpqY in complex with trehalose analogue YB-04. RCSB Protein Data Bank. <https://www.rcsb.org/structure/unreleased/8JAA>. Deposited 5 May 2023.
- B. Zhang, J. X. Liang, Z. H. Rao, Crystal structure of *Mycobacterium tuberculosis* LpqY in complex with trehalose analogue YB-06. RCSB Protein Data Bank. <https://www.rcsb.org/structure/unreleased/8JAB>. Deposited 5 May 2023.
- B. Zhang, J. X. Liang, Z. H. Rao, Crystal structure of *Mycobacterium tuberculosis* LpqY in complex with trehalose analogue YB-16. RCSB Protein Data Bank. <https://www.rcsb.org/structure/unreleased/8JAC>. Deposited 5 May 2023.
- B. Zhang, J. X. Liang, Z. H. Rao, Crystal structure of *Mycobacterium tuberculosis* LpqY in complex with trehalose analogue YB-17. RCSB Protein Data Bank. <https://www.rcsb.org/structure/unreleased/8JAD>. Deposited 5 May 2023.